Role of the pressure transmitting medium on the pressure effects in DWCNTs

B. Anis[1], F. Börrnert[2], M. H. Rümmeli[2], and C. A. Kuntscher[*,1]

[1] Experimentalphysik 2, Universität Augsburg, 86159 Augsburg, Germany
[2] IFW Dresden, P. O. Box 270116, 01171 Dresden, Germany

[*] Corresponding author: e-mail christine.kuntscher@physik.uni-augsburg.de, Phone: +49 (0)821 598 3315, Fax: +49 (0)821 598 3411

1 Introduction The superior and fascinating mechanical properties of carbon nanotubes are ascribed to the strong sp^2 covalent bonds of the carbon atom network [1]. The axial Young's modulus of single-walled carbon nanotubes (SWCNTs) was expected from many theoretical studies [2–4] to be $\geq$1 TPa. However, the carbon nanotubes bulk crystals behave as soft materials because they are bound by weak van der Waals forces [5]. Furthermore, high-pressure studies on the mechanical properties of SWCNTs propose that at a critical pressure a modification of the nanotube's cross-section from circular to oval or elliptical occurs and that SWCNTs collapse at high pressure [6–8]. It has been demonstrated that the homogeneous filling of the SWCNT cavity with an inner wall, forming what is called a double-walled carbon nanotube (DWCNT), stabilizes the outer tube [8–13]. In contrast, filling SWCNTs with C_{70} or iodine molecules, which is considered as a case of inhomogeneous filling, leads to the destabilization of the nanotubes [8, 10, 11, 14, 15]. This was attributed to the inhomogeneous interaction, i.e., van der Waals forces, between the nanotube wall and the inner filler.

Recently, we carried out a high-pressure optical spectroscopy study on the mechanical stability of DWCNTs using nitrogen as pressure transmitting medium (PTM) [9]. In comparison to SWCNTs, the pressure-induced shifts of the optical transitions in the outer tubes of DWCNTs are much smaller below 10 GPa, signaling the stabilization of the outer tube by the inner tube filling. Additionally, the two anomalies at the critical pressures $P_{c1} \approx$ 3 GPa and $P_{c2} \approx$ 7 GPa observed in SWCNTs are suppressed in DWCNTs due to the stabilization effect, and only one anomaly at $P_d \approx$ 12 GPa is observed.

In general, optical spectroscopy is a powerful technique to characterize the electronic band structure in terms of the energy position and spectral weight of the excited optical transitions. As demonstrated recently, the optical response is capable of monitoring small pressure-induced deformations of the tubular cross-section, as the characteristic van Hove singularities in the density of states in SWCNTs are very sensitive to such deformations [16, 17]. Furthermore, it has been shown that the PTM plays an important role for the pressure-induced effects in carbon nanotubes [18].

Here, we present the results of a high-pressure optical spectroscopy study on DWCNTs using nitrogen, argon, and alcohol-mixture as PTM. The results are compared to those for SWCNTs. Our findings show that the PTM greatly influences the pressure effects on the optical transitions, i.e., pressure-induced shifts and anomalies.

2 Experimental DWCNTs were prepared from highly filled C_{60}-peapods: The SWCNTs [Carbon Solutions, Inc. (Type P2, average diameter 1.4 nm)] were filled with C_{60} molecules using the gas phase method described in Ref. [19]. The caps of the SWCNTs were opened by heat treatment at 575 °C for 30 min. Weighted amounts of SWCNTs and fullerene were degassed under dynamic vacuum at 200 °C for 24 h. Then both samples were sealed in a quartz tube under vacuum and heated at 750 °C for 5 days continuously. The non-reacted fullerene was removed by heating the sample at 700 °C under dynamic vacuum for 3 h. The C_{60}-peapods were transformed to DWCNTs by heating the peapods at 1250 °C for 24 h under dynamic vacuum. Free-standing films of SWCNTs and DWCNTs for transmission spectroscopy measurements were prepared from Triton X-100 suspension [20].

The samples were characterized in different preparation stages with a JEOL JEM-2010F transmission electron microscope retrofitted with two CEOS third-order spherical aberration correctors for the objective lens (CETCOR) and the condenser system (CESCOR). The microscope was operated using an electron acceleration voltage of 80 kV to reduce knock on damage. More details about the synthesis and characterization of the samples can be found in Ref. [21]. The diameter of the inner and outer tube in the DWCNT bundles amount to $d_{\text{inner}} \approx 0.80$ nm and $d_{\text{outer}} \approx 1.45$ nm, as estimated from the HRTEM images and Raman spectroscopy [21].

Transmission spectra of the nanotube films were measured at room temperature in the energy range 3500–20 000 cm^{-1} with the resolution 4 cm^{-1} using a Bruker IFS 66v/S Fourier transform infrared spectrometer in combination with an infrared microscope (Bruker IR Scope II) with a 15× Cassegrain objective. For the pressure generation a Syassen–Holzapfel type [22] diamond anvil cell (DAC) was used. The culet size of the diamond anvils is 400 μm. Both top and bottom diamond anvil are perfectly aligned to each other. By using an electrical discharge drilling machine, a 150 μm hole was drilled in a stainless steel gasket, which served as the sample chamber. For the pressure measurements a small piece of the free-standing carbon nanotubes film was carefully placed inside the gasket hole with a few ruby balls for pressure determination. Liquid nitrogen, argon, or alcohol-mixture served as PTM. The intensity $I_s(\omega)$ of the radiation transmitted through the sample placed in the DAC and the intensity $I_{\text{ref}}(\omega)$ of the radiation transmitted through the PTM in the DAC were measured. From $I_s(\omega)$ and I_{ref} (ω) the transmittance and absorbance spectra were calculated according to $T(\omega) = I_s(\omega)/I_{\text{ref}}(\omega)$ and $A(\omega) = -\log_{10} T(\omega)$, respectively.

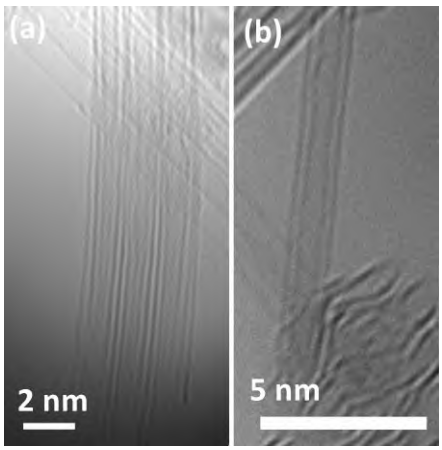

Figure 1 HRTEM image of (a) a bundle of DWCNTs derived from C_{60}-peapods and (b) a single DWCNT.

3 Results and discussion

3.1 Electron microscopy Figure 1a shows the formation of DWCNTs from C_{60}-peapods after heat treatment at 1250 °C for 24 h under dynamic vacuum. Figure 1b shows only one DWCNT to confirm the formation of the inner tubes inside the SWCNTs. Based on the HRTEM images, we estimate a filling ratio of >95%.

3.2 Optical spectroscopy of SWCNTs and DWCNTs under pressure Figures 2 and 3 show the background-subtracted absorbance spectra as a function of pressure for SWCNTs and DWCNTs films, respectively, using (a) nitrogen, (b) argon, and (c) alcohol-mixture (4:1 methanol:ethanol) as PTM. The insets of Figs. 2 and 3 show the absorbance spectra of SWCNTs and DWCNTs at the lowest pressure together with the total fitting curve and the Lorentz contributions. The absorption bands S_{ii} and M_{ii} correspond to the i-th optical transitions in the semiconducting and metallic SWCNTs, respectively. The optical properties of the free-standing SWCNTs and DWCNTs at ambient conditions are explained in detail in our previous works [9, 21]. It is clear that the absorption bands at the lowest pressure are broadened and the fine-structure due to different tube diameters is smeared out, as compared to the free-standing films (see Ref. [9, 21]). In the further discussion, only the strong Lorentz contributions will be considered. In the case of SWCNTs, we observe only one strong contribution for

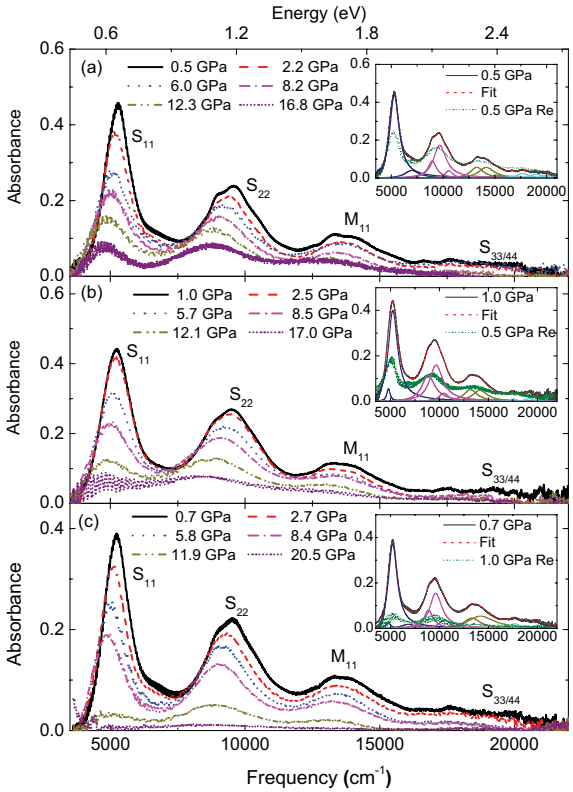

Figure 2 Background-subtracted absorbance spectra of SWCNTs as a function of pressure, using (a) nitrogen, (b) argon, and (c) alcohol-mixture as PTM. The insets in (a–c) depict the absorbance spectrum at the lowest pressure during pressure increase together with the various Lorentzian contributions, and the absorbance spectrum at the lowest pressure during pressure release, in the case of nitrogen, argon, and alcohol-mixture as PTM, respectively.

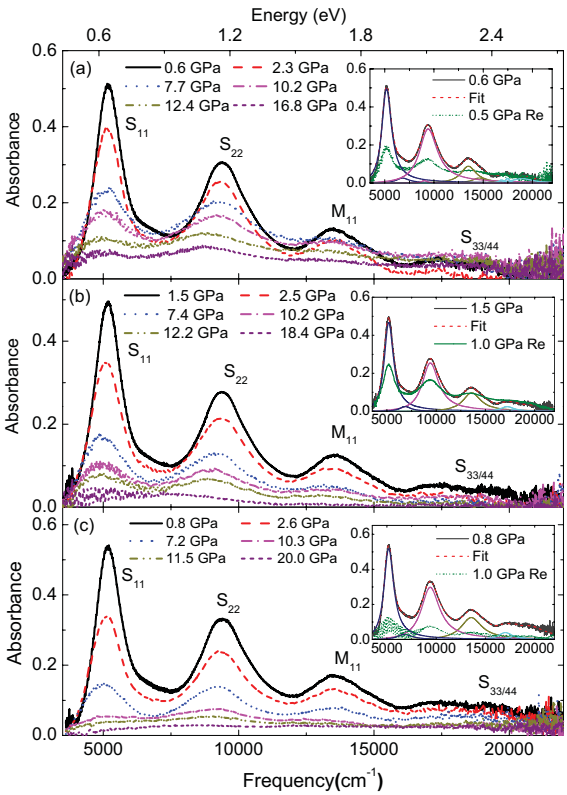

Figure 3 Background-subtracted absorbance spectra of DWCNTs as a function of pressure, using (a) nitrogen, (b) argon, and (c) alcohol-mixture as PTM. The insets in (a–c) depict the absorbance spectrum at the lowest pressure during pressure increase together with the various Lorentzian contributions, and the absorbance spectrum at the lowest pressure during pressure release, in the case of nitrogen, argon, and alcohol-mixture as PTM, respectively.

the S_{11} band and two strong contributions for the S_{22} and M_{11} bands, which are marked by $S_{22}(1)$, $S_{22}(2)$, $M_{11}(1)$, and $M_{11}(2)$, respectively. In comparison, in the case of DWCNTs, we observe only one strong contribution for the S_{11}, S_{22}, and M_{11} absorption bands.

With increasing pressure all absorption bands for both SWCNT and DWCNT films red-shift, broaden, and lose spectral weight (see Figs. 2 and 3). The redshift is generally ascribed to σ^*–π^* hybridization and symmetry breaking [20, 23, 24]. When nitrogen is being used as PTM, all optical transitions S_{11}, S_{22}, and M_{11} are resolvable up to the highest applied pressure (see Figs. 2a and 3a). In case of argon as PTM, all the optical transitions are resolvable up to ≈12 GPa only (see Figs. 2b and 3b). For pressures above 12 GPa, the optical transitions become very broad. Furthermore, all the optical transitions are resolvable only up to ≈10 GPa in the case of alcohol-mixture as PTM (see Figs. 2c, and 3c). Above 10 GPa all the absorption bands are completely smeared out.

Figures 4 and 5 depict the relative energy shifts of the Lorentz contributions as a function of pressure for SWCNTs and DWCNTs, respectively. For the SWCNT films under pressure using nitrogen as PTM (see Fig. 4a), three anomalies in the relative pressure-induced shifts are observed at P_{c1}≈3 GPa, P_{c2}≈7 GPa, and P_{c3}≈13 GPa, followed by a plateau. As criterium for the values of the critical pressures we use the 2nd derivative of the evolution of E_{ii} with pressure (not shown). The shaded gray bars in Fig. 4 mark the pressure regime in which the anomalies are observed, with an error bar of ±0.5 GPa. According to earlier results and theoretical predictions [16, 25–33], we interpret the anomaly at P_{c1} as a structural phase transition from a circular to an oval shape. The anomaly at P_{c2} signals a more drastic change in the tubes' cross-section from oval to race-track or peanut-type shape [7–9]. The plateau with an onset at P_{c3}≈13 GPa indicates a saturation of the pressure-induced deformation and hybridization effects above this pressure. According to our recent pressure investigations on SWCNTs [9] and a high-pressure Raman study [10], we interpret the behavior of the SWCNTs above 13 GPa in terms of the collapse of the tubes. The rapid increase in the shifts above 11 GPa indicate the onset of the collapse, which is completed at P_{c3}. The proposed sequence of structural deformations in SWCNTs is illustrated in Fig. 6a–d.

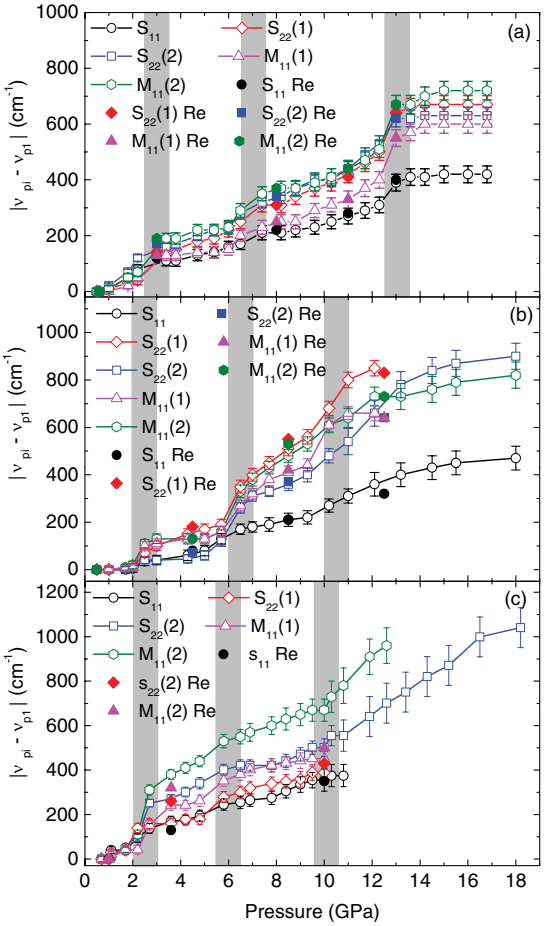

Figure 4 Relative energy shift of the optical transitions as a function of pressure in SWCNTs using (a) nitrogen, (b) argon, and (c) alcohol-mixture as pressure transmitting medium. The shift was calculated as the difference between the absorption frequency of the contribution ν_{pi} at a pressure pi, and the absorption frequency ν_{p1} at the lowest pressure value $p1$. All the contributions during pressure release are marked as S_{ii} (Re) and M_{ii} (Re) for both semiconducting and metallic tubes, respectively. The shaded gray bars mark the pressure regime in which the anomalies are observed, as discussed in the text.

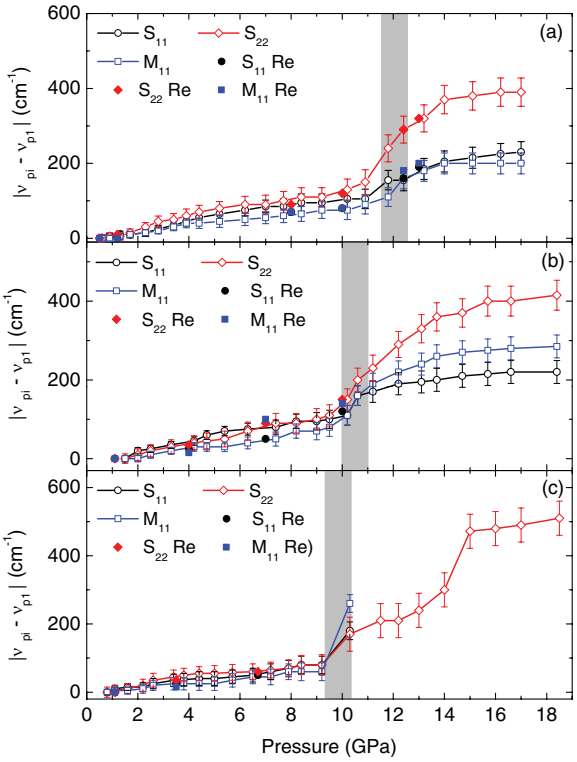

Figure 5 Relative energy shift of the optical transitions as a function of pressure in DWCNTs using (a) nitrogen, (b) argon, and (c) alcohol-mixture as pressure transmitting medium. The shift was calculated as the difference between the absorption frequency of the contribution ν_{pi} at a pressure pi, and the absorption frequency ν_{p1} at the lowest pressure value $p1$. All the contributions during pressure release are marked as S_{ii} (Re) and M_{ii} (Re) for both semiconducting and metallic tubes, respectively. The shaded gray bars mark the pressure regime in which the anomalies are observed, as discussed in the text.

To clarify the influence of the PTM on the mechanical stability of SWCNTs, we show in Fig. 4b and c the relative pressure-induced energy shifts of the Lorentz contributions, using argon and alcohol-mixture as PTM, respectively. The same criterium for determining the critical pressure values as for nitrogen as PTM has been used. In the case of argon, the anomalies in the pressure-induced shifts are lowered to $P_{c1}\approx 2.5$ GPa, $P_{c2}\approx 6.5$ GPa, and $P_{c3}\approx 10.5$ GPa. Above P_{c3} all the optical transitions S_{11}, S_{22}, and M_{11} become very broad and each can be fitted with one Lorentzian contribution. Also the relative energy shifts are higher than the corresponding shifts, when nitrogen is being used as PTM. The broadening of the absorption bands and the lower critical pressures are due to the lower hydrostaticity level of argon compared to nitrogen as PTM [34]. In the case of alcohol-mixture (see Fig. 4c), the anomalies in the pressure-induced shifts are lowered to $P_{c1}\approx 2.5$ GPa, $P_{c2}\approx 6.0$ GPa. Furthermore, some contributions, e.g., $M_{11}(2)$, shift much stronger than others, e.g., S_{11}. Above ≈ 10 GPa, all the absorption bands are smeared out except the $S_{22}(2)$ and $M_{11}(2)$ optical transitions. Both transitions are highly redshifted with a very large error bar because of the broadening, and the shifts do not saturate at high pressure. Alcohol-mixture is a hydrostatic PTM below 10 GPa but becomes quasi-hydrostatic above 10 GPa due to solidification [34]. We suggest that above 10 GPa the SWCNTs are completely collapsed in this case.

Figure 5a shows the relative energy shifts of the optical transitions S_{11}, S_{22}, and M_{11} in the DWCNTs bundles using nitrogen as PTM. Compared to SWCNTs, one notices that the redshift of the absorption bands is very small, with a linear pressure coefficient in the range ~ 9 to 15 $cm^{-1}\,GPa^{-1}$. According to our pervious work on DWCNTs [9], we interpret the small redshift of the absorption bands in terms of the reduction of the σ^*–π^* hybridization and symmetry breaking effects in the outer tubes of the DWCNTs. This finding

signals the mechanical stabilization of the outer tube by the inner tube.

Above ~12 GPa, the relative energy shifts of the absorption bands in the DWCNT bundles steeply increase and seem to saturated at higher pressure (see Fig. 5a). This behavior signals strong pressure-induced alterations in the electronic properties of the outer tube at a critical pressure $P_d \approx 12$ GPa related to tubular deformation, which are completed at ~14 GPa. Several Raman studies reported higher critical pressures for the structural transition of the outer tube in DWCNTs as compared to SWCNTs, and this was attributed to the structural support of the outer tube by the inner tube [10, 33, 35].

Interestingly, a very recent high-pressure Raman spectroscopy study on the same type of sample, i.e., C_{60}-peapod-derived DWCNT sample with similar inner and outer tube diameters, and using paraffin oil as PTM found anomalies in the G-bands at similar pressures. The findings were interpreted in terms of the onset of the collapse of the DWCNTs at 12 GPa and its completion at 15 GPa. The lower value of the critical pressure as compared to CVD-grown DWCNTs was attributed to the inhomogenous filling [11]. It was furthermore suggested that the collapse of DWCNTs occurs in different steps. From the molecular dynamics simulations by Gadagkar et al. [33] the tubes cross-sections remain nearly circular up to a critical pressure, where the tube cross-sections are deformed to an elliptical shape. The critical pressure follows a $1/R_{\text{eff}}^3$ dependence [33], where the effective radius (R_{eff}) of the DWCNT is defined as $1/R_{\text{eff}}^3 = (1/n)\sum_{i=1}^{n}(1/R_i^3)$ with $n = 2$ for DWCNTs. Based on this relation we calculate the effective radius for our DWCNT bundles with $d_{\text{inner}} \approx 0.80$ nm and $d_{\text{outer}} \approx 1.45$ nm, as estimated from the HRTEM images and Raman spectroscopy [21], to $R_{\text{eff}} \approx 0.5$ nm and obtain a critical pressure value of $P_d \approx 11$ GPa according to Ref. [33]. Thus, our experimental finding of a critical pressure $P_d \approx 12$ GPa is in very good agreement with theoretical predictions. We can interpret this anomaly in terms of a discontinuous volume change accompanied by a cross-sections' change to two deformed hexagons [36]. The proposed sequence of structural deformations in DWCNTs is illustrated in Fig.6e and f.

Figure 5b and c shows the relative pressure-induced energy shifts of the optical transitions in DWCNTs using argon and alcohol-mixture as PTM, respectively. In the case of argon, the critical pressure P_d is lowered to ≈10.5 GPa. Above P_d the relative energy shifts are slightly higher than the corresponding shifts, when nitrogen is being used as PTM. This could be attributed to the lower hydrostaticity level of argon compared to nitrogen as PTM [34]. Furthermore, in the case of alcohol-mixture, all the absorption bands are completely smeared out above 10 GPa. Above 10 GPa the DWCNTs might be collapsed due to the solidification of alcohol-mixture [34]. Interestingly, the deformation process of the DWCNTs seems to be more complicated according to our data, consisting of several steps, similar to the findings in Ref. [10].

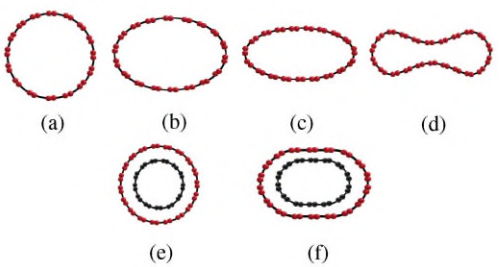

Figure 6 Proposed sequence of structural deformation of SWCNTs (a–d) and of DWCNTs (e–f).

It is important to note that according to our results filling of the nanotubes with nitrogen, argon, or alcohol-mixture does not prevent the pressure-induced anomalies in the electronic transitions due to tubular deformation, in contradiction to earlier reports [37].

Finally, we comment on the reversibility of the pressure-induced structural changes. For both SWCNTs and DWCNTs the pressure-induced frequency shifts of the optical transitions are reversible upon pressure release (see the insets of Figs. 2a–c and 3a–c). However, one notices a loss in intensity of the original absorbance value, namely, up to ≈ 60% in the case of nitrogen and argon and ≈ 85% in the case of alcohol mixture. The irreversible changes indicate that a fraction of the tubes has been permanently damaged during pressure loading, with a loss of the characteristic features in their density of states. In the case of alcohol mixture, the greater damage of tubes is due to the non-hydrostaticity of the alcohol mixture above 10 GPa [34].

4 Conclusions Compared to empty SWCNTs, the redshift of the absorption bands in DWCNTs is smaller and follows an approximately linear behavior for nitrogen as PTM, signaling the stabilization of the outer tube by the inner tube regarding its electronic properties. An anomaly in the pressure-induced shifts of the absorption bands in DWCNTs at around $P_d \approx 12$ GPa indicates the deformation of the outer tubes to deformed hexagons. SWCNTs exhibit three anomalies in the pressure-induced shifts of the absorption bands at $P_{c1} \approx 3$ GPa, $P_{c2} \approx 7$ GPa, and $P_{c3} \approx 13$ GPa for nitrogen as PTM. Due to the lower hydrostaticity level of argon compared to nitrogen as PTM, the anomalies in the pressure-induced shifts are lowered to $P_{c1} \approx 2.5$ GPa, $P_{c2} \approx 6.5$ GPa, and $P_{c3} \approx 10.5$ GPa and $P_d \approx 11$ GPa in the case of SWCNTs and DWCNTs, respectively. In the case of alcohol-mixture as PTM, above ≈10 GPa the SWCNTs and DWCNTs seem to be completely collapsed due to the non-hydrostaticity of the alcohol-mixture above 10 GPa. The pressure-induced alterations of the absorption bands are reversible regarding their frequency position but not completely reversible regarding their intensity, indicating that a fraction of the tubes has been permanently damaged under high pressure load for nitrogen and argon as PTM. The higher damage of the tubes in the case of alcohol mixture can be explained by its non-hydrostaticity above 10 GPa because of solidification.

Acknowledgements This work is financially supported by the DFG (KU1432/3-2, RU1540/8-1), the DAAD, and the Egyptian Government.

References

[1] A. Jorio, R. Saito, G. Dresselhaus, and M. S. Dresselhaus, Raman Spectroscopy in Graphene Related Systems (Wiley-VCH Verlag GmbH, Weinheim, 2011).
[2] A. Krishnan, E. Dujardin, T. W. Ebbesen, P. N. Yianilos, and M. M. J. Treacy, Phys. Rev. B **58**, 14013 (1998).
[3] E. Hernández, C. Goze, P. Bernier, and A. Rubio, Phys. Rev. Lett. **80**, 4502 (1998).
[4] J. P. Lu, Phys. Rev. Lett. **79**, 1297 (1997).
[5] S. Kawasaki, Y. Matsuoka, T. Yokomae, Y. Nojima, F. Okino, H. Touhara, and H. Kataura, Carbon **43**, 37 (2005).
[6] S. Lebedkin, K. Arnold, O. Kiowski, F. Hennrich, and M. M. Kappes, Phys. Rev. B **73**, 094109 (2006).
[7] M. Yao, Z. Wang, B. Liu, Y. Zou, S. Yu, W. Lin, Y. Hou, S. Pan, M. Jin, B. Zou, T. Cui, G. Zou, and B. Sundqvist, Phys. Rev. B **78**, 205411 (2008).
[8] C. Caillier, D. Machon, A. San-Miguel, R. Arenal, G. Montagnac, H. Cardon, M. Kalbac, M. Zukalova, and L. Kavan, Phys. Rev. B **77**, 125418 (2008).
[9] B. Anis, K. Haubner, F. Börrnert, L. Dunsch, M. H. Rümmeli, and C. A. Kuntscher, Phys. Rev. B **86**, 155454 (2012).
[10] A. L. Aguiar, E. B. Barros, R. B. Capaz, A. G. Souza Filho, P. T. C. Freire, J. M. Filho, D. Machon, C. Caillier, Y. A. Kim, H. Muramatsu, M. Endo, and A. San-Miguel, J. Phys. Chem. C **115**, 5378 (2011).
[11] A. L. Aguiar, A. San-Miguel, E. B. Barros, M. Kalbáč, D. Machon, Y. A. Kim, H. Muramatsu, M. Endo, and A. G. Souza Filho, Phys. Rev. B **86**, 195410 (2012).
[12] R. Pfeiffer, H. Kuzmany, C. Kramberger, C. Schaman, T. Pichler, H. Kataura, Y. Achiba, J. Kürti, and V. Zólyomi, Phys. Rev. Lett. **90**, 225501 (2003).
[13] P. Puech, H. Hubel, D. J. Dunstan, R. R. Bacsa, C. Laurent, and W. S. Bacsa, Phys. Rev. Lett. **93**, 095506 (2004).
[14] L. Alvarez, J. L. Bantignies, R. Le Parc, R. Aznar, J. L. Sauvajol, A. Merlen, D. Machon, and A. San Miguel, Phys. Rev. B **82**, 205403 (2010).
[15] A. Sohi and R. Naghdabadi, Acta Mater. **55**, 5483 (2007).
[16] K. Thirunavukkuarasu, F. Hennrich, K. Kamarás, and C. A. Kuntscher, Phys. Rev. B **81**, 045424 (2010).
[17] C. A. Kuntscher, A. Abouelsayed, K. Thirunavukkuarasu, and F. Hennrich, Phys. Status Solidi B **247**, 2789 (2010).
[18] A. Abouelsayed, K. Thirunavukkuarasu, F. Hennrich, and C. A. Kuntscher, J. Phys. Chem. C **114**, 4424 (2010).
[19] B. W. Smith, R. M. Russo, S. B. Chikkannanavar, F. Stercel, and D. E. Luzzi, Mater. Res. Soc. Symp. Proc. **706**, Z3.13.1 (2002).
[20] Z. Wu, Z. Chen, X. Du, J. M. Logan, J. Sippel, M. Nikolou, K. Kamaras, J. R. Reynolds, D. B. Tanner, A. F. Hebard, and A. G. Rinzler, Science **305**, 1273 (2004).
[21] B. Anis, M. Fischer, M. Schreck, K. Haubner, L. Dunsch, and C. A. Kuntscher, Phys. Status Solidi B **249**, 2345 (2012).
[22] G. Huber, K. Syassen, and W. B. Holzapfel, Phys. Rev. B **15**, 5123 (1977).
[23] J. C. Charlier, P. Lambin, and T. W. Ebbesen, Phys. Rev. B **54**, R8377 (1996).
[24] G. Liu, X. Wang, J. Chen, and H. Lu, Phys. Status Solidi B **245**, 689 (2008).
[25] R. B. Capaz, C. D. Spataru, P. Tangney, M. L. Cohen, and S. G. Louie, Phys. Status Solidi B **241**, 3352 (2004).
[26] S. P. Chan, W. L. Yim, X. G. Gong, and Z. F. Liu, Phys. Rev. B **68**, 075404 (2003).
[27] M. H. F. Sluiter and Y. Kawazoe, Phys. Rev. B **69**, 224111 (2004).
[28] J. A. Elliott, J. K. W. Sandler, A. H. Windle, R. J. Young, and M. S. P. Shaffer, Phys. Rev. Lett. **92**, 095501 (2004).
[29] M. Hasegawa and K. Nishidate, Phys. Rev. B **74**, 115401 (2006).
[30] U. D. Venkateswaran, A. M. Rao, E. Richter, M. Menon, A. Rinzler, R. E. Smalley, and P. C. Eklund, Phys. Rev. B **59**, 10928 (1999).
[31] M. J. Peters, L. E. McNeil, J. P. Lu, and D. Kahn, Phys. Rev. B **61**, 5939 (2000).
[32] J. Sandler, M. S. P. Shaffer, A. H. Windle, M. P. Halsall, M. A. Montes-Morán, C. A. Cooper, and R. J. Young, Phys. Rev. B **67**, 035417 (2003).
[33] V. Gadagkar, P. K. Maiti, Y. Lansac, A. Jagota, and A. K. Sood, Phys. Rev. B **73**, 085402 (2006).
[34] S. Klotz, J. C. Chervin, P. Munsch, and G. L. Marchand, J. Phys. D, Appl. Phys. **42**, 075413 (2009).
[35] S. You, M. Mases, I. Dobryden, A. A. Green, M. C. Hersam, and A. V. Soldatov, High Press. Res. **31**, 186 (2011).
[36] X. Yang, G. Wu, and J. Dong, Appl. Phys. Lett. **89**, 113101 (2006).
[37] A. Merlen, N. Bendiab, P. Toulemonde, A. Aouizerat, A. San Miguel, J. L. Sauvajol, G. Montagnac, H. Cardon, and P. Petit, Phys. Rev. B **72**, 035409 (2005).